Supplement of Earth Syst. Sci. Data, 16, 2297–2316, 2024
https://doi.org/10.5194/essd-16-2297-2024-supplement

Supplement of

A 30 m annual cropland dataset of China from 1986 to 2021

Ying Tu et al.

Correspondence to: Bing Xu (bingxu@tsinghua.edu.cn)

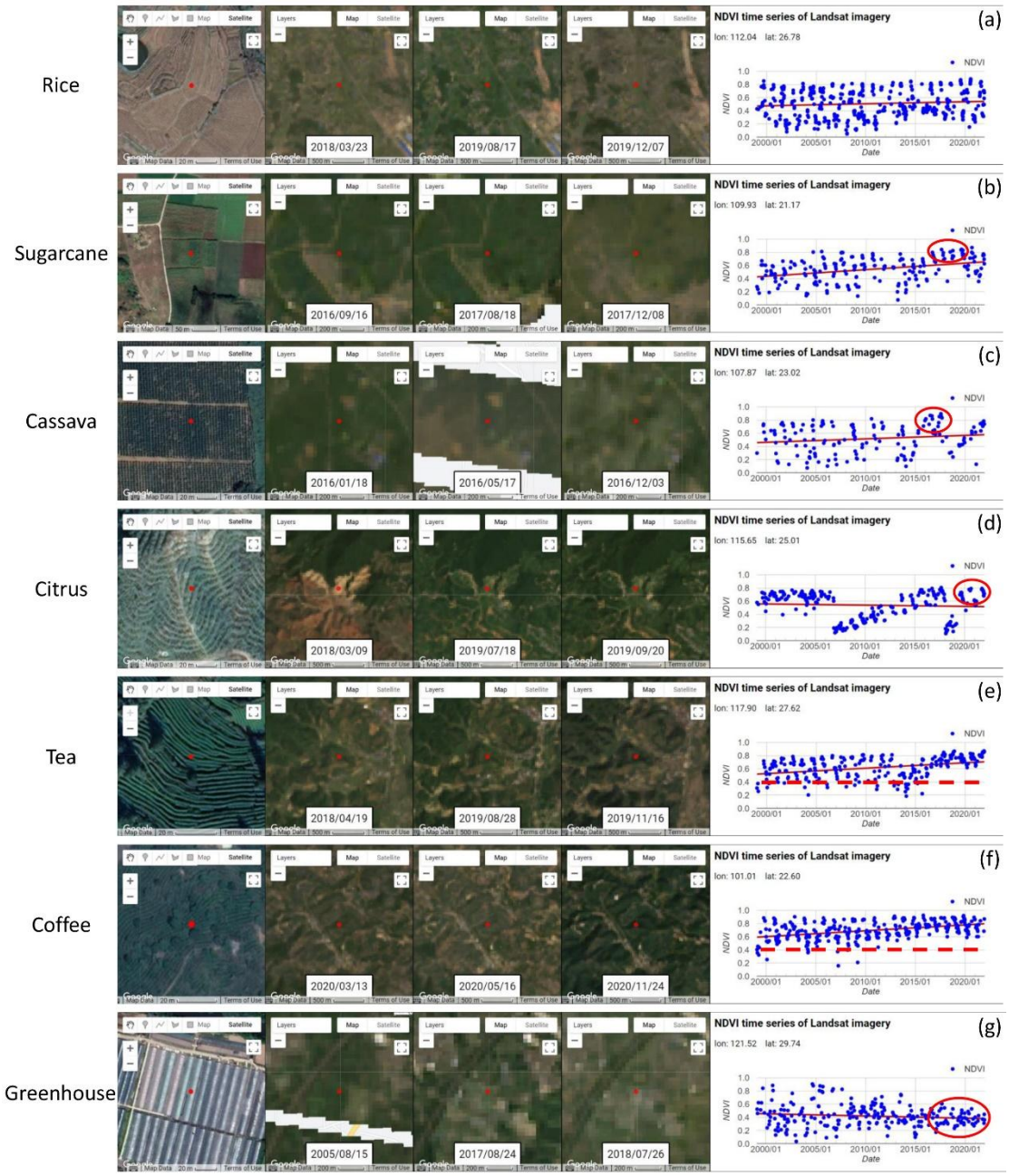

Figure S1. Comparisons of satellite images and NDVI time series between annual cropland defined in this study and other crops. (a) Rice fields in Hengyang, Hunan. (b) Sugarcane plantation in Zhanjiang, Guangdong. (c) Cassava crops in Nanning, Guangxi. (d) Citrus trees in Ganzhou, Jiangxi. (e) Tea gardens in Wuyishan, Fujian. (f) Coffee trees in Pu'er, Yunnan. (g) Recent greenhouse construction in Ningbo, Zhejiang. The red circles and dashed lines in subfigures (b-g) highlight the NDVI differences between other crops and the cropland defined in this study. All the figures are generated using © Google Earth Engine.

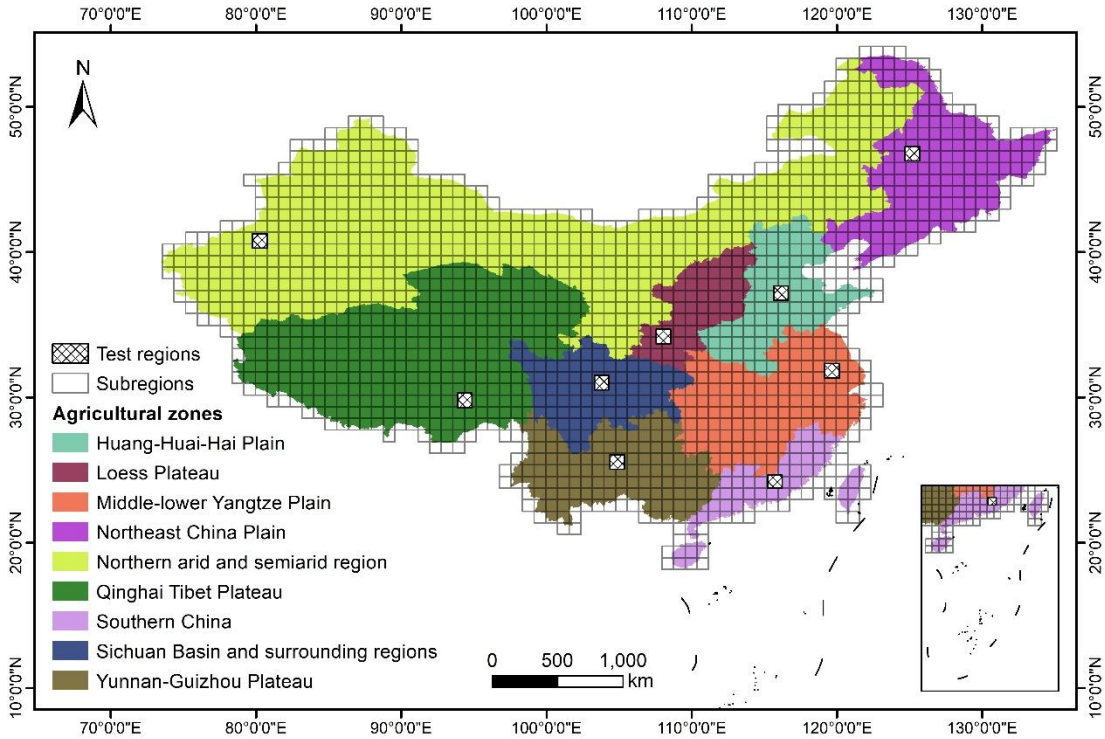

Figure S2. Divisions of the study area. Annual cropland classification is performed within each 0.8°×0.8° subregion. Test regions with a size of 100 ×100 km are used to find the best LandTrendr arguments for each agricultural zone.

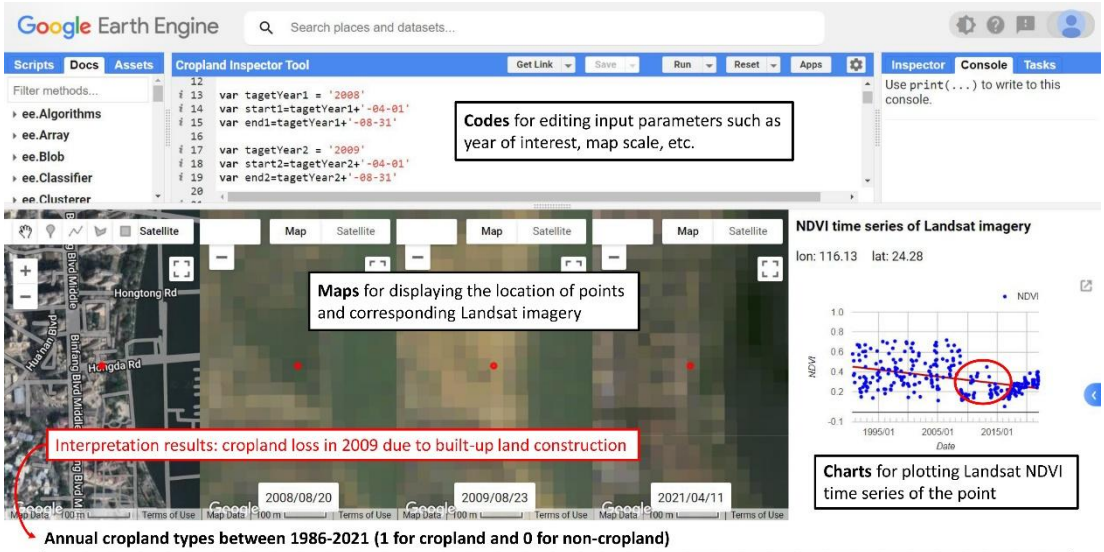

Annual cropland types between 1986-2021 (1 for cropland and 0 for non-cropland)

Point Id	86	87	88	89	90	91	92	93	94	95	96	97	98	99	00	01	02	03	04	05	06	07	08	09	10	11	12	13	14	15	16	17	18	19	20	21
29	1	1	1	1	1	1	1	1	1	1	1	1	1	1	1	1	1	1	1	1	1	1	1	0	0	0	0	0	0	0	0	0	0	0	0	0

Figure S3. An example of the sample interpretation process using the developed Cropland Inspector Tool on © Google Earth Engine. The location was covered by croplands before 2009 but converted to built-up areas since then, of which changes were clearly shown in Landsat images and NDVI time series.

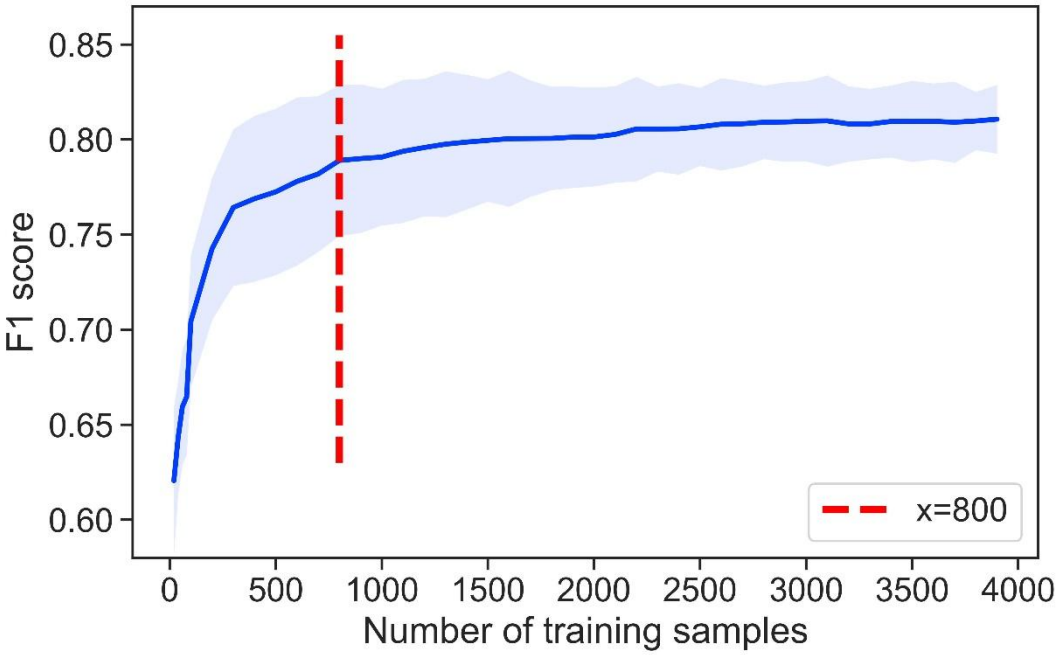

Figure S4. Mean F1 score of annual cropland classification results under different training sample sizes.

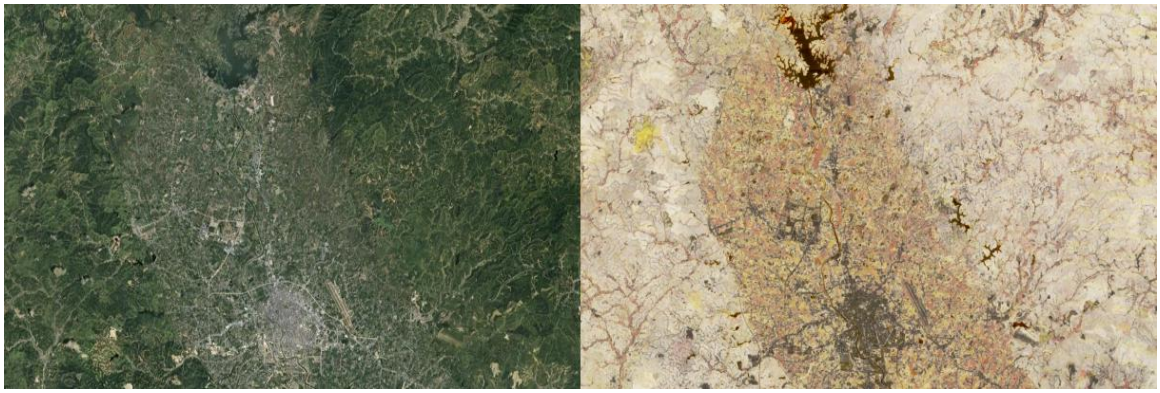

Figure S5. A comparison of a true color Landsat imagery displayed (left) and a corresponding NDVI composite imagery (with 90th, 50th, and 10th percent quantile of one-year values as the RGB channels) on the right. The Landsat imagery is provided by USGS with free access.

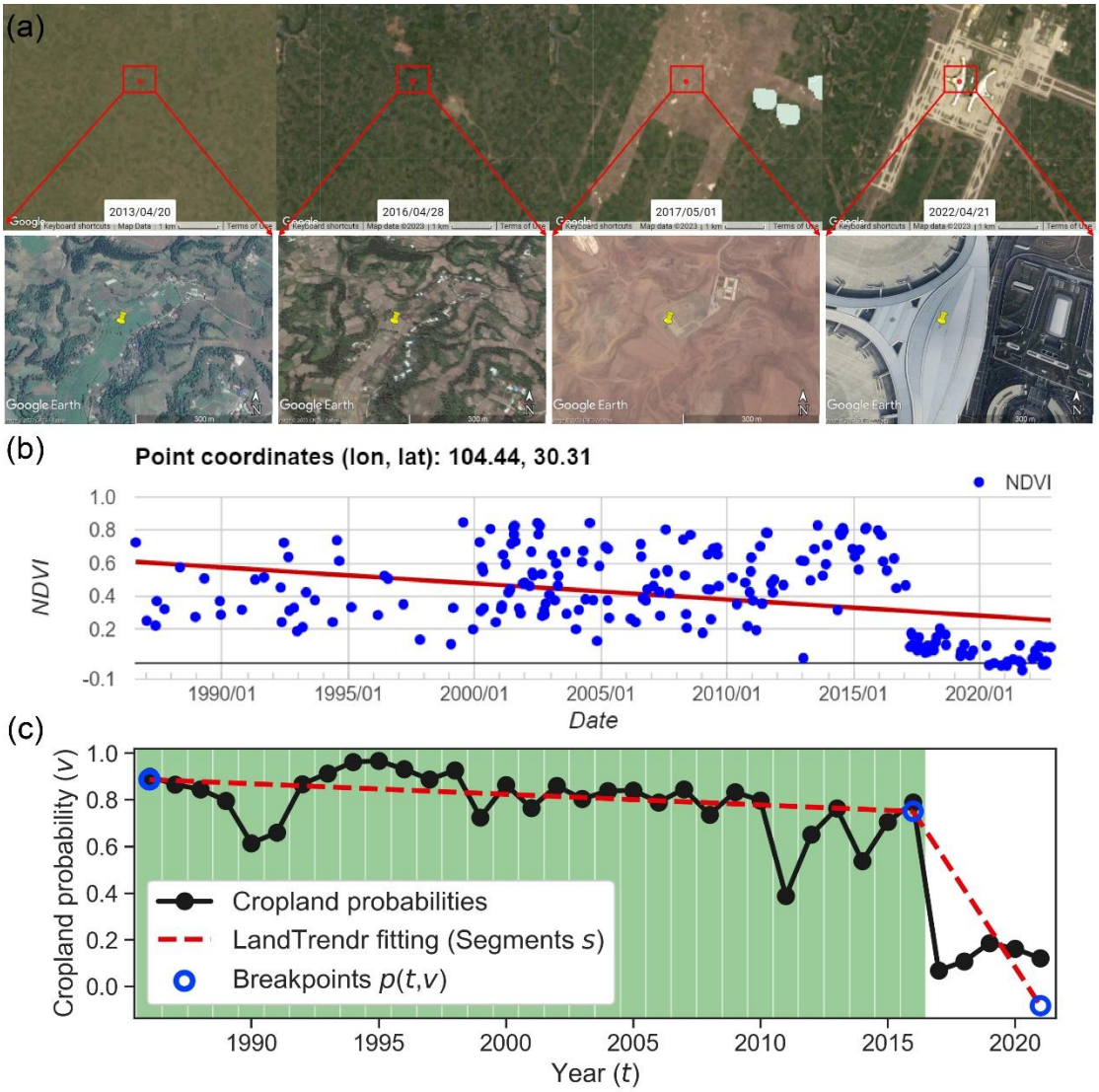

Figure S6. An illustration of cropland to urban land conversion in Chengdu, Sichuan. (a) Landsat and © Google Earth high-resolution images over time. (b) NDVI time series for the selected point of interest. (c) Estimated cropland probabilities, LandTrendr segmentations, and final mapping outcomes (green: cropland, white: non-cropland) for the selected point. All the Landsat images are freely provided by USGS.

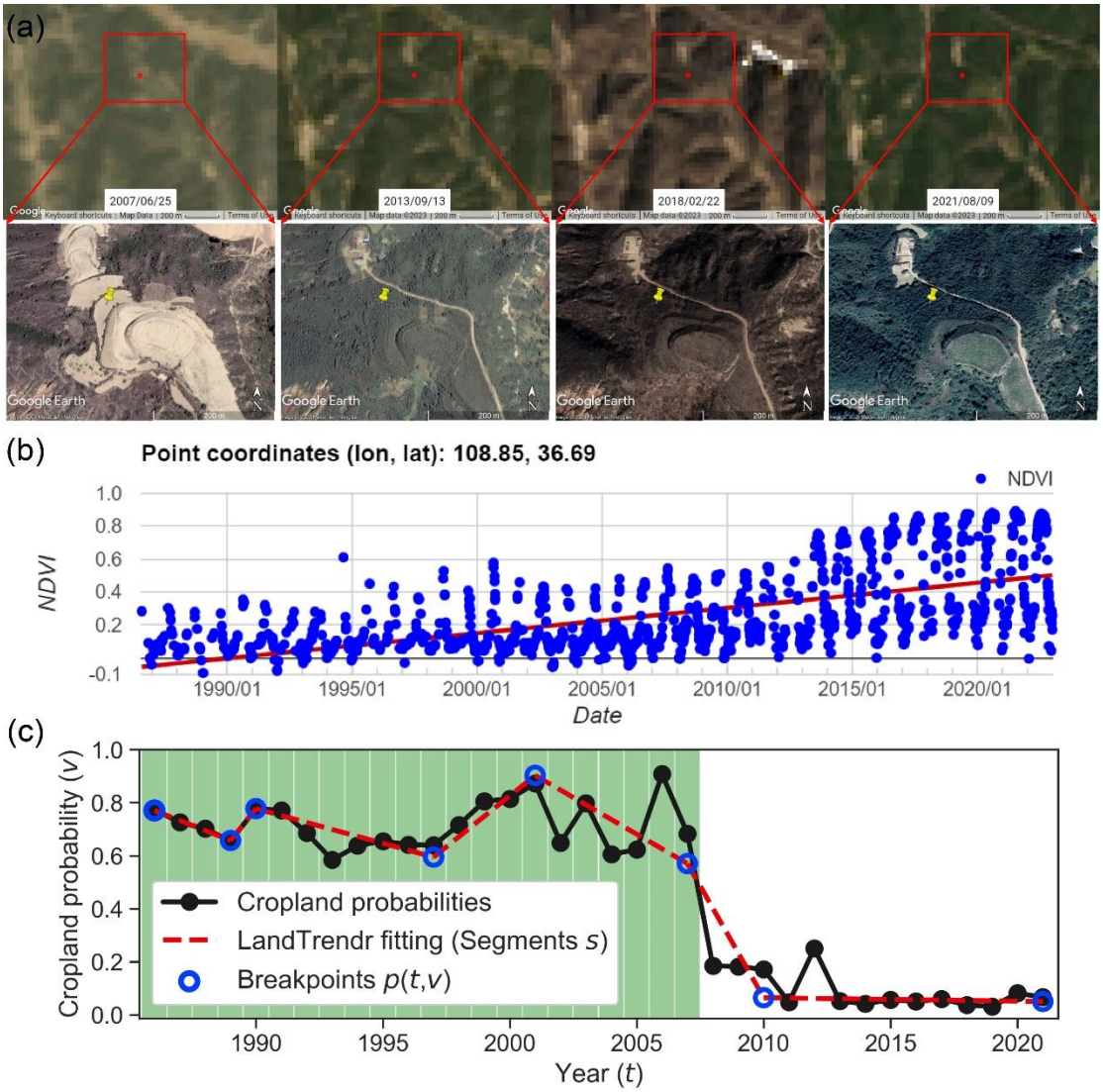

Figure S7. An illustration of cropland to forest conversion in Yan'an, Shaanxi. (a) Landsat and © Google Earth high-resolution images over time. (b) NDVI time series for the selected point of interest. (c) Estimated cropland probabilities, LandTrendr segmentations, and final mapping outcomes (green: cropland, white: non-cropland) for the selected point. All the Landsat images are freely provided by USGS.

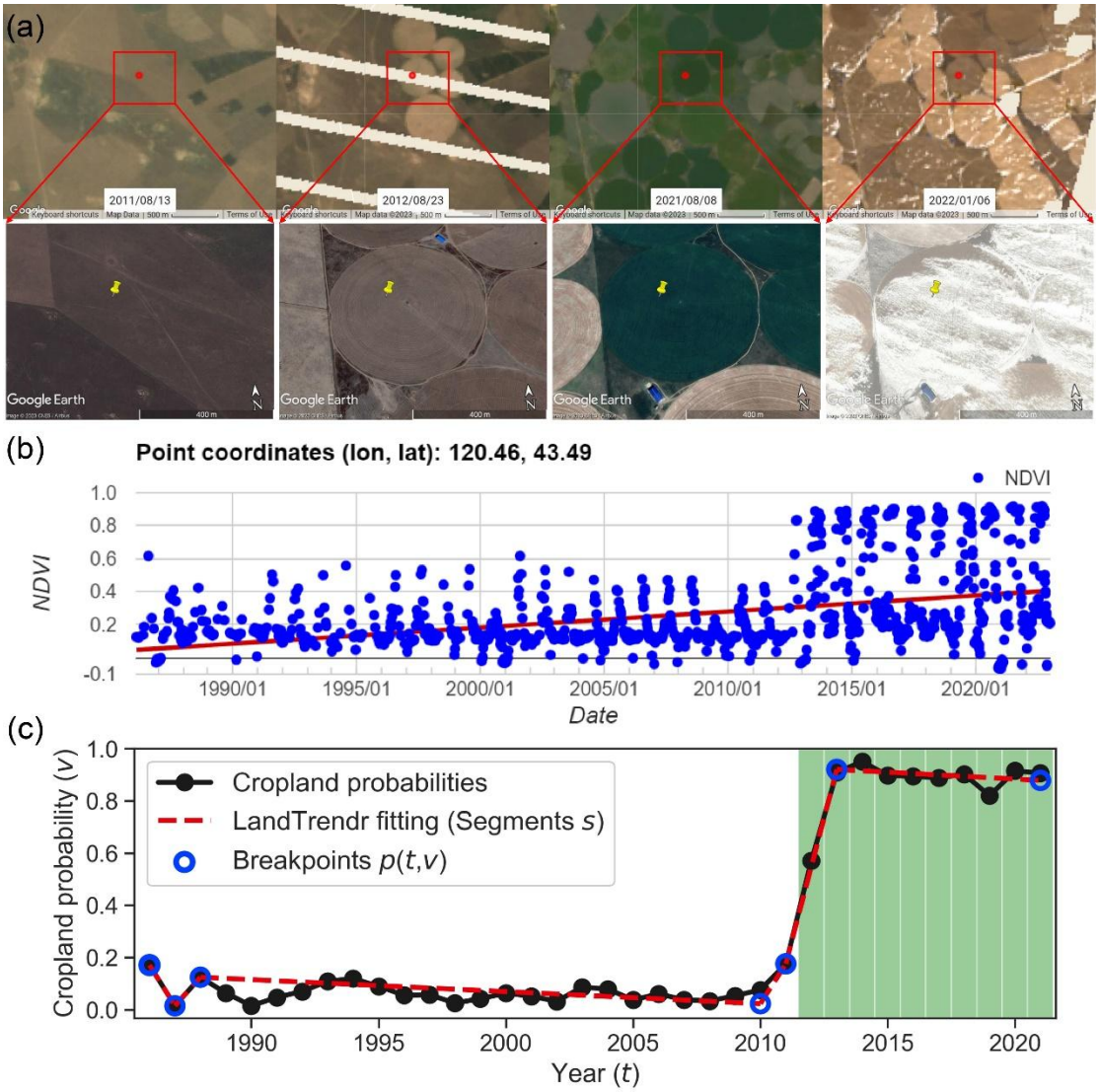

Figure S8. An illustration of grass to cropland conversion in Chifeng, Inner Mongolia. (a) Landsat and © Google Earth high-resolution images over time. (b) NDVI time series for the selected point of interest. (c) Estimated cropland probabilities, LandTrendr segmentations, and final mapping outcomes (green: cropland, white: non-cropland) for the selected point. All the Landsat images are freely provided by USGS.

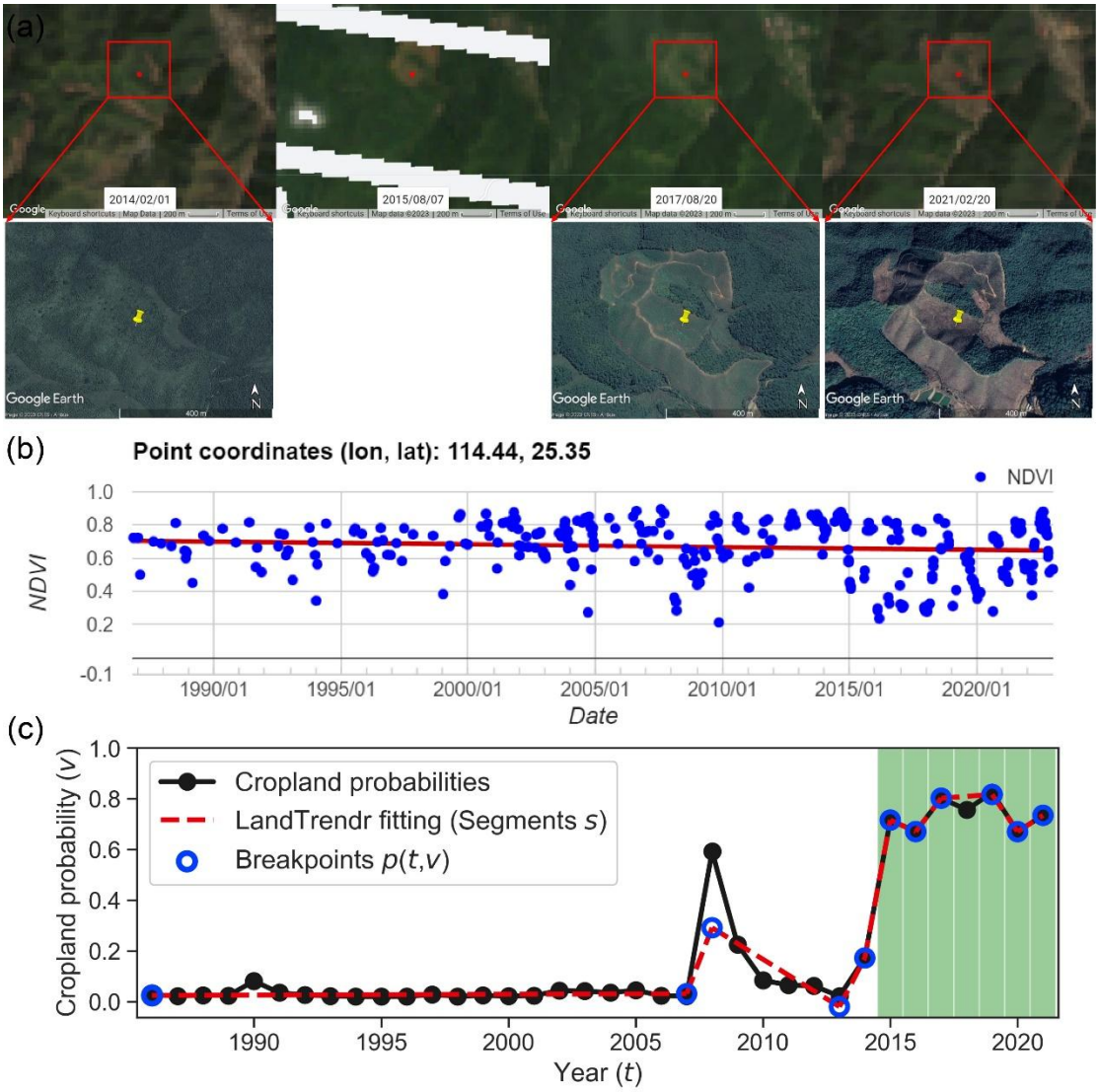

Figure S9. An illustration of forest to cropland conversion in Shaoguan, Guangdong. (a) Landsat and © Google Earth high-resolution images over time. (b) NDVI time series for the selected point of interest. (c) Estimated cropland probabilities, LandTrendr segmentations, and final mapping outcomes (green: cropland, white: non-cropland) for the selected point. All the Landsat images are freely provided by USGS.

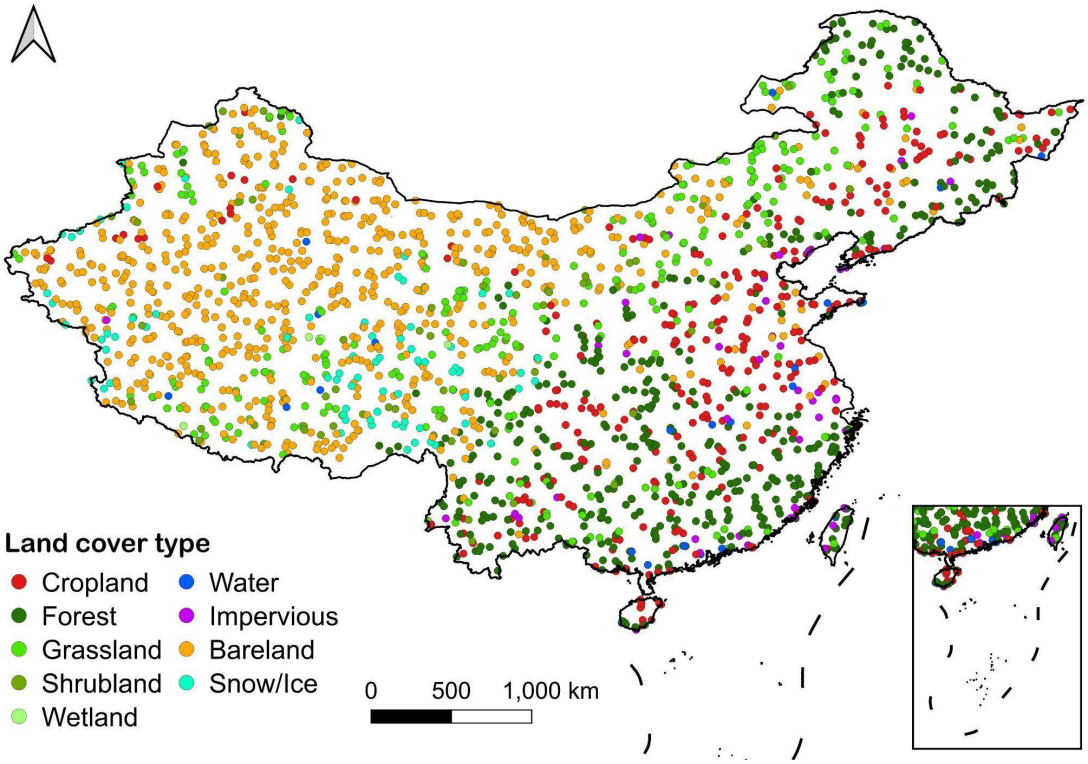

Figure S10. Spatial distribution of global land cover validation sample set (GLCVSS) in China.

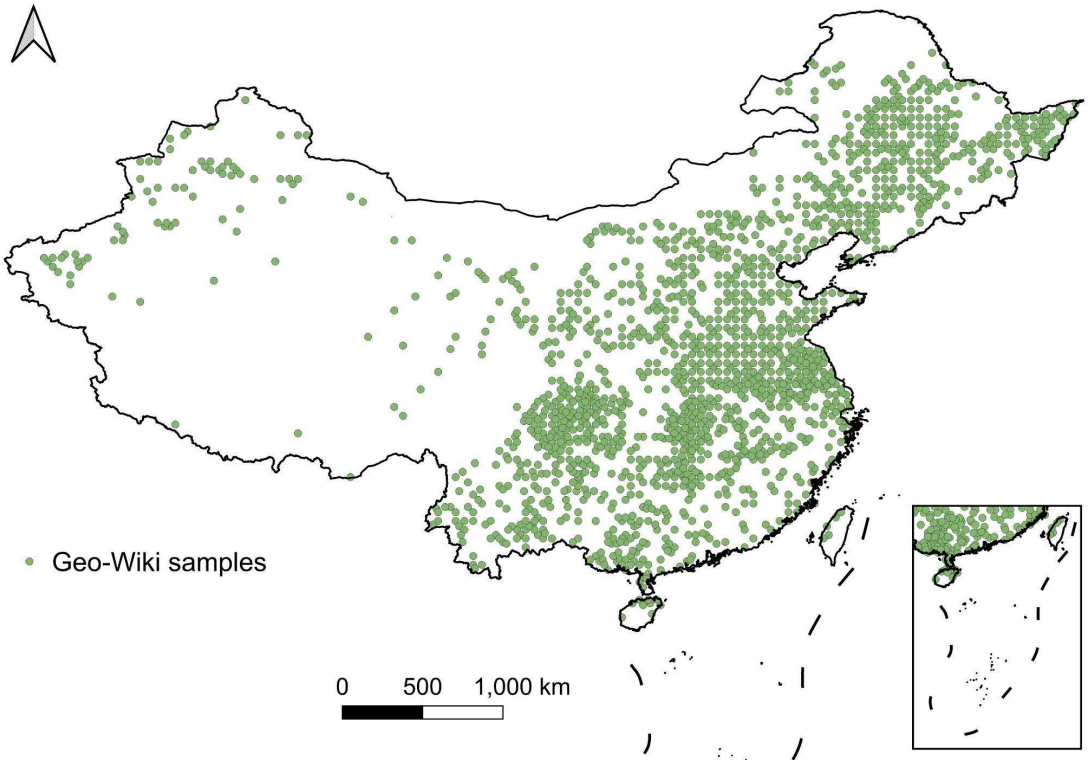

Figure S11. Spatial distribution of GeoWiki cropland samples in China.

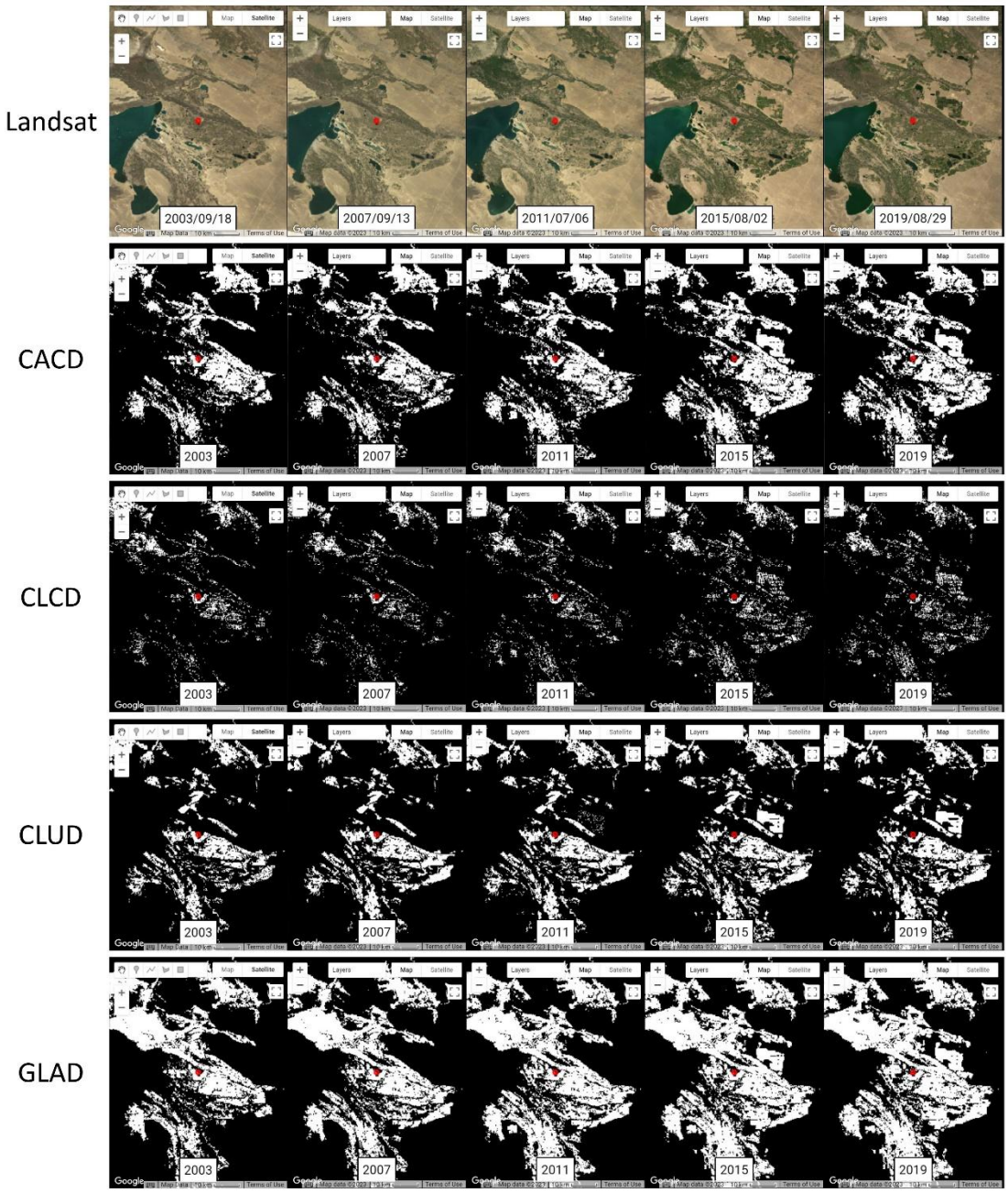

Figure S12. Comparisons of Landsat images and cropland products across years in Altay, Xinjiang, with cropland shown in white and non-cropland shown in black. All the figures are generated using © Google Earth Engine.

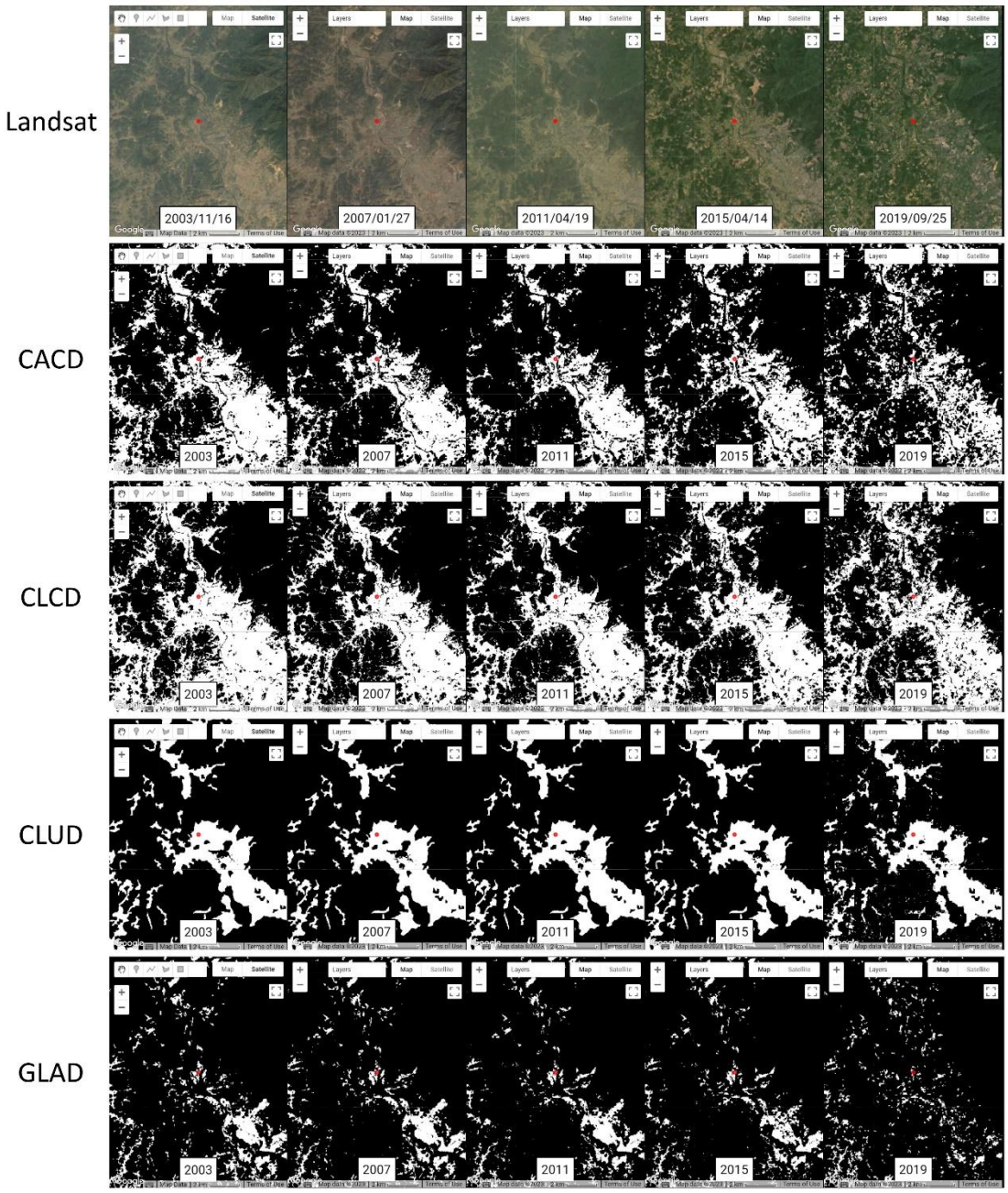

Figure S13. Comparisons of Landsat images and cropland products across years in Liuzhou, Guangxi, with cropland shown in white and non-cropland shown in black. All the figures are generated using © Google Earth Engine.

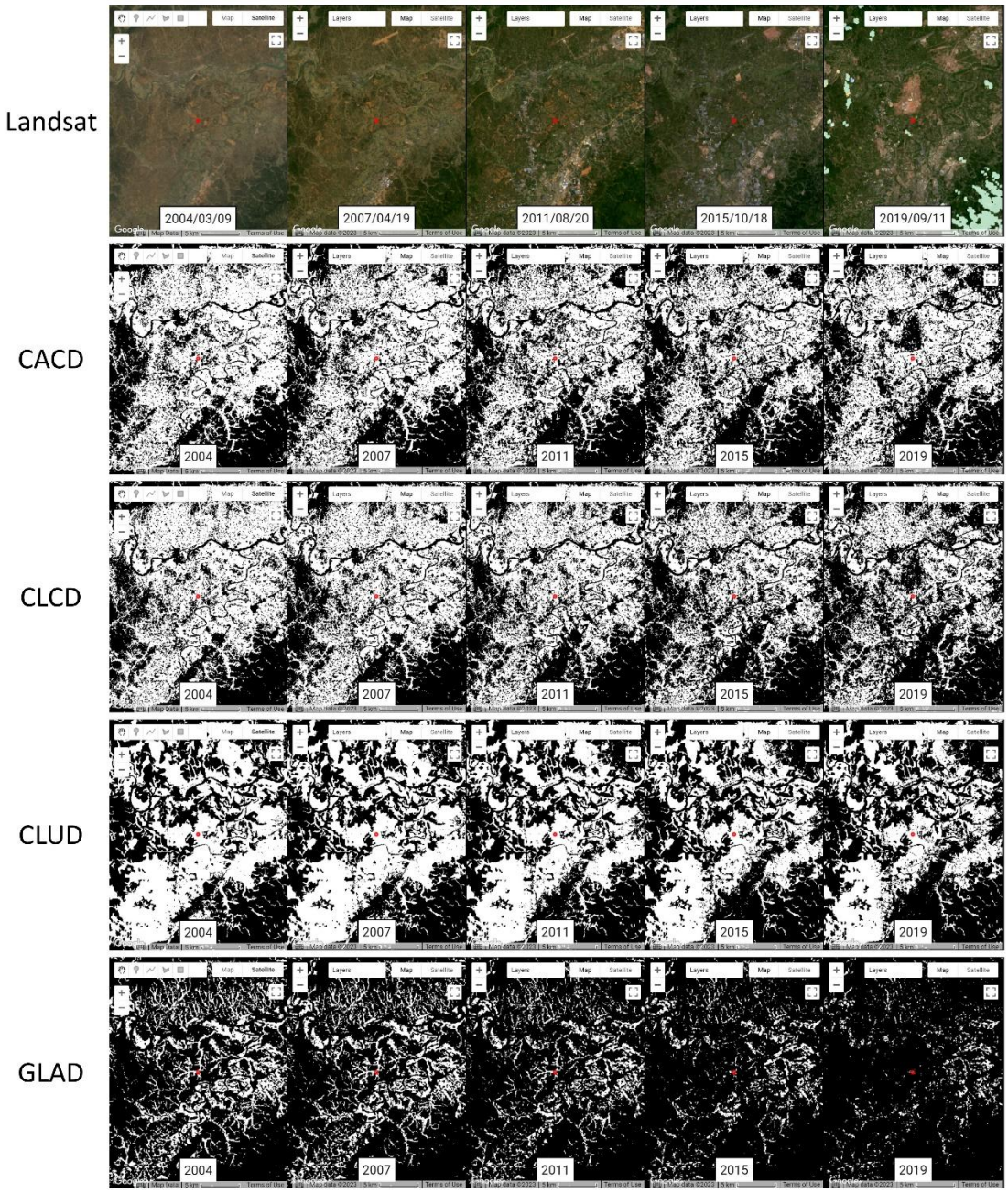

Figure S14. Comparisons of Landsat images and cropland products across years in Ganzhou, Jiangxi, with cropland shown in white and non-cropland shown in black. All the figures are generated using © Google Earth Engine.

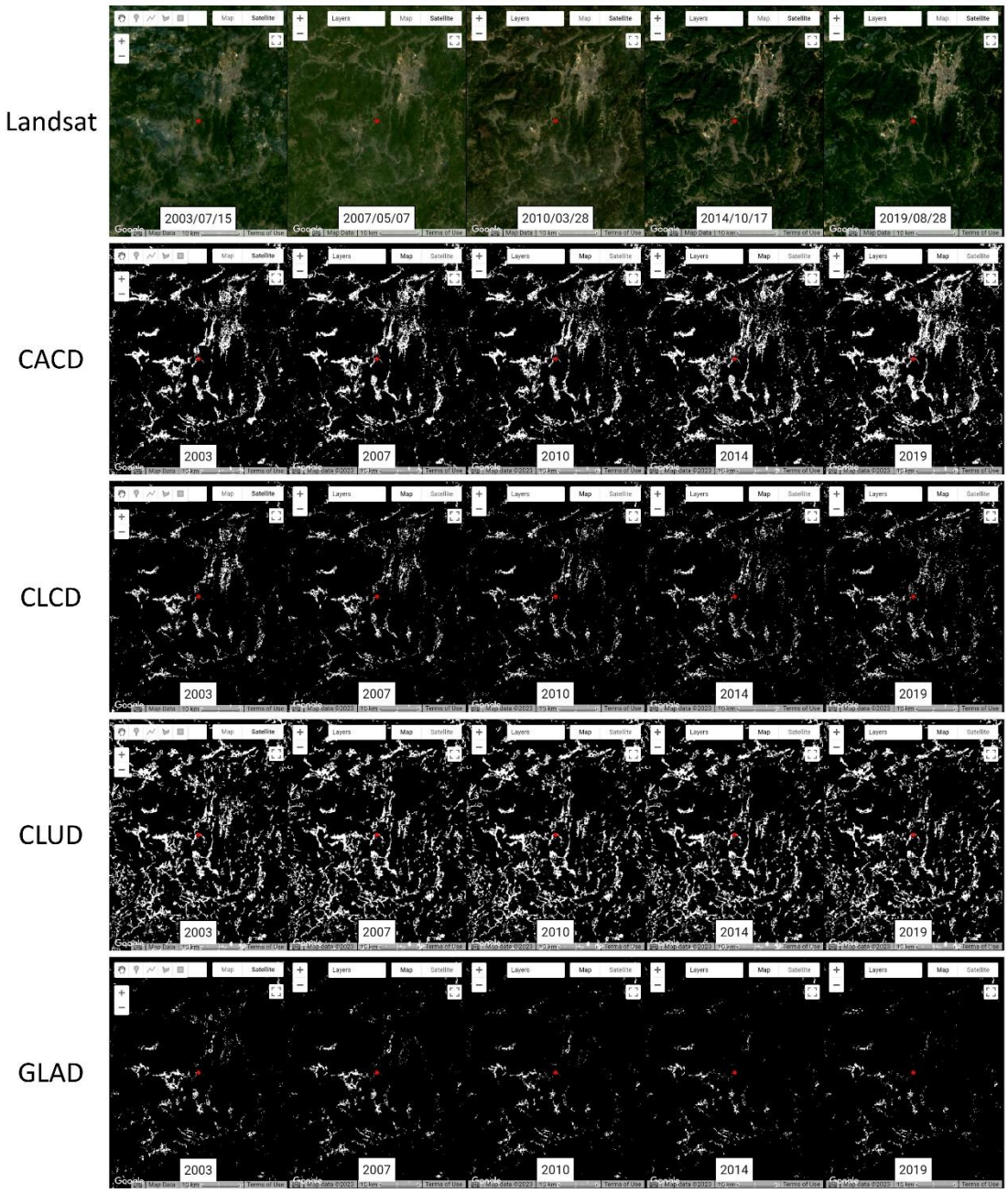

Figure S15. Comparisons of Landsat images and cropland products across years in Longyan, Fujian, with cropland shown in white and non-cropland shown in black. All the figures are generated using © Google Earth Engine.

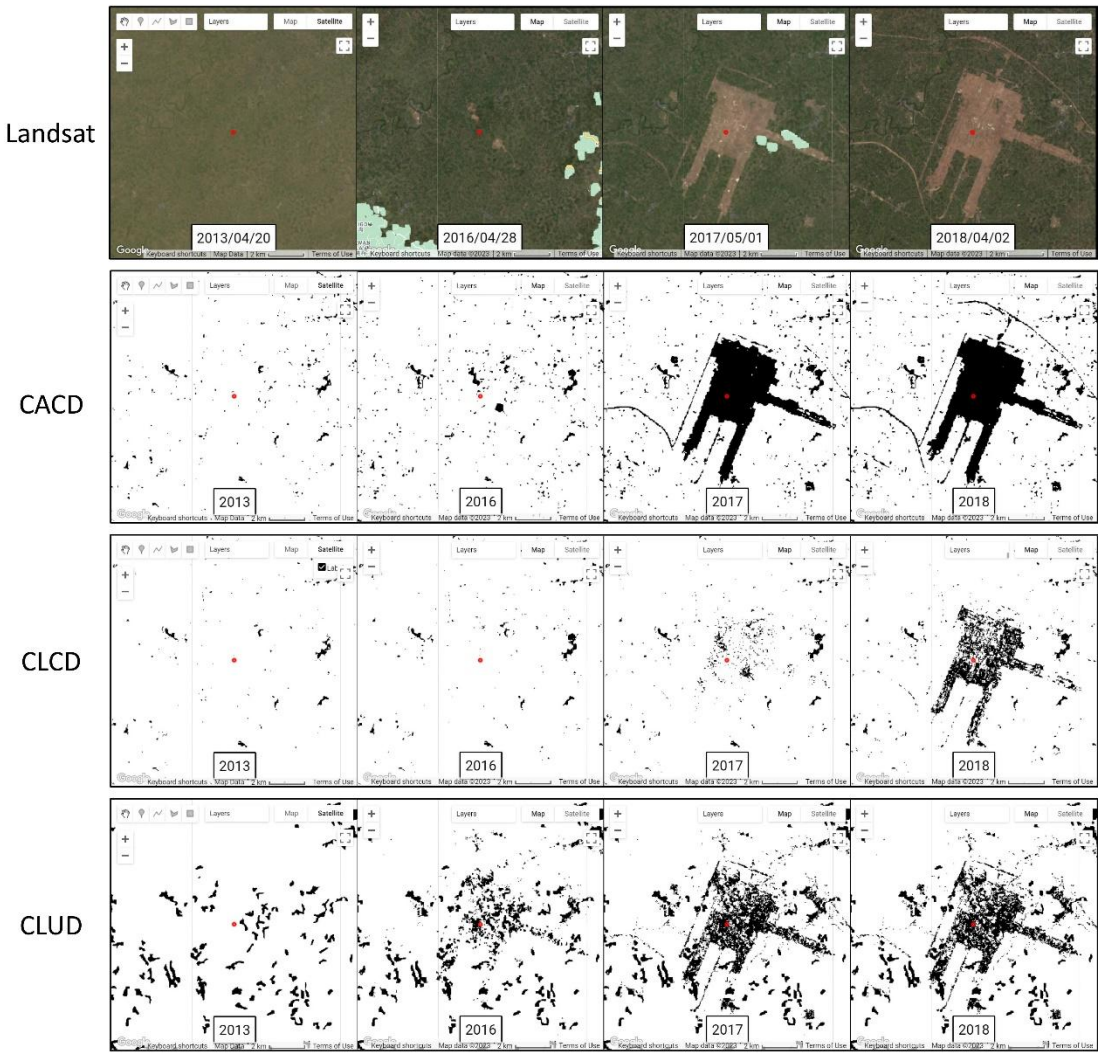

Figure S16. Comparisons of Landsat images and cropland products across years in Chengdu, Sichuan, with cropland shown in white and non-cropland shown in black. All the figures are generated using © Google Earth Engine.

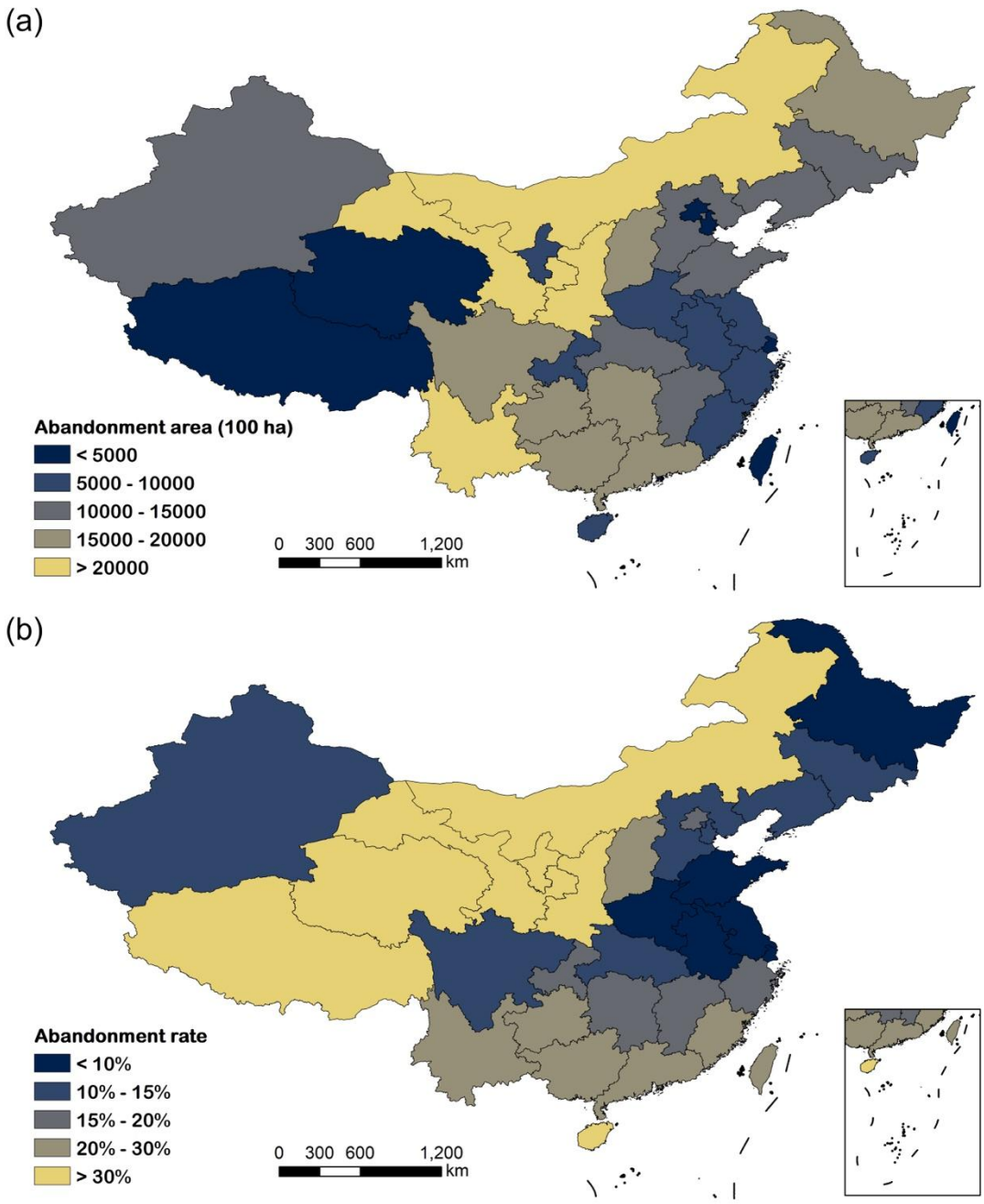

Figure S17. Provincial cropland abandonment in China between 1990-2015 of (a) area and (b) rate.

Table S1. A summary of the nine agricultural zones in China: their geographical and climatic conditions, growing seasons, cropping patterns, and major crops

Agricultural zones	**Geographical and climatic conditions**	**Growing seasons**	**Cropping patterns**	**Major crops**
Huang-Huai-Hai Plain	The largest alluvial plain of China being at the intersection of humid winds from the Pacific and dry winds from the interior of the Asian continent. Land is fertile and suitable for agricultural activity.	April to September	Double cropping	Wheat, maize, sorghum, millet, peanuts, sesame seed, cotton
Loess Plateau	Has a continental monsoon climate. Winters are cold and dry, and most rainfall occurs during the summer. Annual precipitation is ~400 mm. Most areas are hills and plateaus covered by loess, with serious soil erosion.	May to September	Single cropping	Wheat, maize, millet, corn, sorghum
Middle-lower Yangtze Plain	Centered on the extensive lowland plains of east-central China. Experiences a temperate climate with warm springs, hot summers, cool autumns, and relatively cold winters for the latitude.	April to October	Tripple cropping	Rice, maize, rapeseed, sweet potato, pea
Northeast China Plain	Under the humid continental climate zone with a hot rainy summer and cold dry winter. Suitable for mechanized farming, with thick and fertile soil and extensive amounts of arable land.	May to September	Single cropping	Wheat, maize, soybean, millet, sorghum, sugar beet
Northern arid and semiarid region	Has an arid desert climate. Has abundant light energy resources and good heat conditions, but precipitation is low, and sandstorms and alkalinization are severe	June to September	Single or double cropping	Wheat, maize, soybean, oat, potato, melon, cotton, sugar beet
Qinghai Tibet Plateau	Belongs to the alpine plateau climate. Covered mainly by plateaus and mountains with 4000 meters above sea level. Difficult for cereal planting and only suitable for grazing.	May to September	Single cropping	Wheat, highland barley, potato
Sichuan Basin and surrounding regions	A lowland region in southwestern China. Experiences a subtropical monsoon climate with warm, hazy summers and chilly winter fog. Frost-free period is of 280-350 days.	April to October	Double or triple cropping	Rice, wheat, maize, red sage, rapeseed
Southern China	The only tropical economic crop planting area in the country. Experiences a subtropical and tropical climate with high temperatures and heavy rainfall particularly during the summer.	March to October	Triple cropping	Rice, maize, potato, sugarcane
Yunnan-Guizhou Plateau	A large mountainous region with rugged terrain. Climate gradually transitions from drier in the southwest to rainier in the northeast - in east-central Yunnan, parts of the Yungui Plateau experience a semi-arid climate, while most of Guizhou is classified as the humid subtropical region.	March to October	Double or triple cropping	Rice, maize, sweet potato, rapeseed

Table S2. Input features of multi-temporal metrics each year for the random forest classifier for estimating annual cropland probabilities.

Category	Feature	Description	Dimension	Source
Spectrum	10th, 25th, 50th, 75th, and 90th percent quantiles of Blue, Green, Red, NIR, SWIR1, and SWIR2 bands of both growing and non-growing seasons	Spectral bands of Landsat data	6*5*2	Landsat
Spectral indices	10th, 25th, 50th, 75th, and 90th percent quantiles of NDVI, NDSI, NDBI, NBR, and EVI indices of both growing and non-growing seasons	Normalized indices derived from spectral bands, which are calculated as: NDVI = (NIR-Red)/(NIR+Red) NDSI = (Green-SWIR1)/(Green+SWIR1) NDBI = (SWIR1-NIR)/(SWIR1+NIR) NBR = (NIR-SWIR1)/(NIR+SWIR2) EVI = 2.5*((NIR-Red)/(NIR+6*Red-7.5*Blue+1))	5*5*2	Landsat
Tasseled cap transformation indices	10th, 25th, 50th, 75th, and 90th percent quantiles of brightness, greenness, and wetness indices of both growing and non-growing seasons	Tasseled cap transformation indices of spectral bands. Coefficients are derived from Crist (1985).	3*5*2	
Topography	Elevation	/	1	SRTM

Noted NIR and SWIR are short for the near-infrared and short-wave bands of Landsat data respectively. NDVI, NDSI, NDBI, NBR, and EVI are abbreviations for the normalized difference vegetation index, the normalized difference snow index, the normalized difference built-up index, the normalized burn ratio, and the enhanced vegetation index, respectively.

Table S3. Ten settings of LandTrendr parameters tested in this study.

Parameter	**Settings**									
	1	2	3	4	5	6	7	8	9	10
maxSegments	6	8	10	8	10	6	8	8	8	8
spikeThreshold	0.9	0.9	0.9	0.5	0.5	0.9	0.9	0.9	0.9	0.9
preventOneYearRecovery	TRUE	TRUE	TRUE	TRUE	TRUE	FALSE	TRUE	TRUE	TRUE	TRUE
recoveryThreshold	0.25	0.25	0.25	0.25	0.25	0.25	0.5	0.75	0.25	0.25
pvalThreshold	0.05	0.05	0.05	0.05	0.05	0.05	0.05	0.05	0.1	0.05
bestModelProportion	0.75	0.75	0.75	0.75	0.75	0.75	0.75	0.75	0.75	0.5

Noted other parameters are set as default as those provided in https://emapr.github.io/LT-GEE/lt-gee-requirements.html.

Table S4. Annual cropland classification results for each test region in the nine agricultural zones (refer to Fig. S2) under different LandTrendr parameter settings.

Agricultural zone	**Parameter settings with the highest F1 score**	**Statistics of F1 scores**		
		Highest	Mean	Std
Huang-Huai-Hai Plain	3	0.89	0.87	0.01
Loess Plateau	4	0.83	0.80	0.04
Middle-lower Yangtze Plain	5	0.80	0.80	0.02
Northeast China Plain	4	0.88	0.87	0.01
Northern arid and semiarid region	6	0.71	0.62	0.06
Qinghai Tibet Plateau	8	0.67	0.59	0.10
Sichuan Basin and surrounding regions	5	0.78	0.76	0.02
Southern China	4	0.69	0.65	0.06
Yunnan-Guizhou Plateau	5	0.75	0.71	0.04

Std: standard deviations.

Table. S5. Definitions of cropland in CACD, CLCD, CLUD, GLAD, and GFSAD.

Product	Cropland definition	Reference
CACD	Defined as a piece of land of 0.25 ha in minimum (minimum width of 30 m) that is sowed/planted and harvestable at least once within the 12 months after the sowing or planting date. This definition excludes: • Perennial crops like sugarcane and cassava • Fruit, tea, and coffee plantations • Greenhouse crops • Small plots such as legumes that do not meet the minimum size criteria of cropland	This study
CLCD	Defined as cultivated lands for crops. Including: mature cultivated land, newly cultivated land, fallow, shifting cultivated land; intercropping land such as crop-fruiter, crop-mulberry, and crop-forest land in which a crop is a dominant species; bottomland and beach that cultivated for at least 3 years.	(Yang and Huang, 2021)
CLUD	Defined as cultivated lands for crops. Including: mature cultivated land, newly cultivated land, fallow, shifting cultivated land; intercropping land such as crop-fruiter, crop-mulberry, and crop-forest land in which a crop is a dominant species; bottomland and beach that cultivated for at least 3 years.	(Xu et al., 2020)
GLAD	Defined as land used for annual and perennial herbaceous crops for human consumption, forage (including hay) and biofuel. Perennial woody crops, permanent pastures and shifting cultivation are excluded from the definition. The fallow length is limited to 4 years for the cropland class.	(Potapov et al., 2022)
GFSAD	Net cropland extent mapped was defined as the sum of the following agricultural croplands: • Cropland that is cultivated and harvested for food, feed, and (or) fiber, one or more times during a 12-month period; • Cropland that is left fallow, even when equipped for agriculture; and • Cropland that is permanently cropped with plantations (for example, orchards, vineyards, coffee, tea, and rubber). Notably, pasture land is not part of the cropland, except for alfalfa in the United States and some other countries.	(Thenkabail et al., 2021)

Noted both CLCD and CLUD were generated based on the China land-use/cover datasets developed by the Chinese Academy of Sciences, which encompassed six primary land cover classes (level-1) and 25 sub-classes (level-2) (Liu et al., 2014; Liu et al., 2005; Liu et al., 2003). Following Yang and Huang (2021) and Xu et al. (2020), we adopted their definition of cropland for the level-1 class.

Table. S6. Pixel-wise accuracy of CACD calculated based on the annual validation samples. F1: F1 score. OA: overall accuracy. Kappa: Kappa coefficient. UA: user's accuracy. PA: producer's accuracy.

Year	F1	OA	UA	PA	Kappa
1986	0.76	0.91	0.77	0.75	0.70
1987	0.76	0.92	0.78	0.75	0.71
1988	0.77	0.92	0.78	0.75	0.71
1989	0.77	0.92	0.78	0.76	0.72
1990	0.76	0.92	0.78	0.75	0.71
1991	0.77	0.92	0.78	0.76	0.72
1992	0.78	0.92	0.78	0.77	0.73
1993	0.77	0.92	0.78	0.77	0.72
1994	0.78	0.92	0.78	0.77	0.73
1995	0.78	0.92	0.79	0.77	0.73
1996	0.78	0.92	0.79	0.77	0.73
1997	0.78	0.92	0.79	0.77	0.73
1998	0.78	0.92	0.79	0.78	0.74
1999	0.79	0.92	0.79	0.79	0.74
2000	0.79	0.93	0.79	0.80	0.75
2001	0.80	0.93	0.79	0.80	0.75
2002	0.79	0.92	0.79	0.80	0.75
2003	0.79	0.92	0.79	0.79	0.74
2004	0.79	0.93	0.79	0.80	0.75
2005	0.80	0.93	0.80	0.80	0.76
2006	0.80	0.93	0.80	0.81	0.76
2007	0.80	0.93	0.80	0.80	0.76
2008	0.80	0.93	0.80	0.81	0.76
2009	0.81	0.93	0.81	0.81	0.77
2010	0.81	0.93	0.80	0.82	0.77
2011	0.82	0.93	0.81	0.82	0.78
2012	0.82	0.94	0.81	0.83	0.78
2013	0.82	0.94	0.81	0.82	0.78
2014	0.82	0.94	0.82	0.82	0.78
2015	0.82	0.94	0.82	0.83	0.79
2016	0.81	0.93	0.80	0.82	0.77
2017	0.81	0.93	0.81	0.81	0.77
2018	0.81	0.93	0.81	0.81	0.77
2019	0.80	0.93	0.80	0.80	0.76
2020	0.80	0.93	0.80	0.80	0.76
2021	0.80	0.93	0.79	0.81	0.76
Mean	0.79±0.02	0.93±0.01	0.79±0.01	0.79±0.02	0.75±0.02

Table. S7. Accuracy of CACD for the year of change under different tolerance years.

Tolerance (years)	Accuracy
0	0.76
±1	0.79
±2	0.81
±3	0.84
±4	0.86
±5	0.87

Supplementary references

Crist, E.P. (1985). A TM Tasseled Cap equivalent transformation for reflectance factor data. *Remote Sensing of Environment, 17*, 301-306

Liu, J., Kuang, W., Zhang, Z., Xu, X., Qin, Y., Ning, J., Zhou, W., Zhang, S., Li, R., Yan, C., Wu, S., Shi, X., Jiang, N., Yu, D., Pan, X., & Chi, W. (2014). Spatiotemporal characteristics, patterns, and causes of land-use changes in China since the late 1980s. *Journal of Geographical Sciences, 24*, 195-210

Liu, J., Liu, M., Tian, H., Zhuang, D., Zhang, Z., Zhang, W., Tang, X., & Deng, X. (2005). Spatial and temporal patterns of China's cropland during 1990–2000: An analysis based on Landsat TM data. *Remote Sensing of Environment, 98*, 442-456

Liu, J., Liu, M., Zhuang, D., Zhang, Z., & Deng, X. (2003). Study on spatial pattern of land-use change in China during 1995–2000. *Science in China Series D: Earth Sciences, 46*, 373-384

Potapov, P., Turubanova, S., Hansen, M.C., Tyukavina, A., Zalles, V., Khan, A., Song, X.-P., Pickens, A., Shen, Q., & Cortez, J. (2022). Global maps of cropland extent and change show accelerated cropland expansion in the twenty-first century. *Nature Food, 3*, 19-28

Thenkabail, P.S., Teluguntla, P.G., Xiong, J., Oliphant, A., Congalton, R.G., Ozdogan, M., Gumma, M.K., Tilton, J.C., Giri, C., Milesi, C., Phalke, A., Massey, R., Yadav, K., Sankey, T., Zhong, Y., Aneece, I., & Foley, D. (2021). Global cropland-extent product at 30-m resolution (GCEP30) derived from Landsat satellite time-series data for the year 2015 using multiple machine-learning algorithms on Google Earth Engine cloud. In, *Professional Paper* (p. 63). Reston, VA

Xu, Y., Yu, L., Peng, D., Zhao, J., Cheng, Y., Liu, X., Li, W., Meng, R., Xu, X., & Gong, P. (2020). Annual 30-m land use/land cover maps of China for 1980–2015 from the integration of AVHRR, MODIS and Landsat data using the BFAST algorithm. *Science China Earth Sciences, 63*, 1390-1407

Yang, J., & Huang, X. (2021). The 30 m annual land cover dataset and its dynamics in China from 1990 to 2019. *Earth System Science Data, 13*, 3907-3925